Journal of Engineering Physics and Thermophysics, Vol. 81, No. 1, 2008

ON THE MECHANISM OF CARBON TRANSPORT TO THE DEPOSITION SURFACE IN A FLOW DISCHARGE REACTOR FOR SYNTHESIS OF CARBON NANOMATERIALS

V. M. Volzhankin, A. V. Krauklis, S. P. Fisenko, and A. I. Shnip

UDC 536.248.2

The process of obtaining structurized carbon nanomaterials in a gas-discharge plasma reactor at atmospheric pressure has been investigated. A mathematical model of this process has been developed based on the hypothesis that free carbon formed in the discharge plasma of this reactor is transported from its discharge zone to the deposition zone in the form of nanoparticles and is deposited on the reactor walls under the action of thermophoresis. A comparison of the results of calculations carried out with this model and the corresponding experimental data has strengthened the indicated hypothesis.

Introduction. The authors of [1, 2] realized a new method of obtaining carbon nanomaterials in an atmospheric-pressure discharge plasma. A characteristic feature of this method is that the carbon material is deposited on the metallic walls of a reactor, located downstream of the discharge zone. It may be suggested with a high degree of probability that it is precisely on these surfaces where nanomaterials are formed and grow; therefore, the solution of the problem on the rate and mechanism of transport of the initial material to the indicated surfaces is of great importance. Note that, at present, the form in which carbon is transported from the discharge zone to the cooling zone — the condensed phase (carbon clusters of the type of C_n) or a gaseous hydrocarbon compound — remains unknown. Our numerous experiments have shown that the necessary condition for the formation of a structurized carbon on the metallic surface of a reactor is the existence of a temperature gradient between the gas flow and this surface. This circumstance suggests that the thermophoresis plays a great role in this process and, therefore, the decomposition of methane in the discharge zone leads to the formation of carbon clusters (or carbon-containing nanoparticles) that are transported by a gas flow to the deposition (or growth) zone and are deposited by the thermophoretic forces on the reactor walls.

For the problems considered below it makes no difference whether these particles are structurized carbon nanomaterials formed in the discharge zone of a reactor or amorphous particles that, when they reach the reactor walls, form carcass carbon structures as a result of the interaction with the iron of the walls by the mechanism described in [3]. The aim of the present work is to calculate the transport of particles under the action of thermophoresis in the deposition zone of a flow reactor and, on the basis of a comparison of theoretical predictions with experimental data, to determine the role of this process in the technology being considered.

Experimental. A carbon nanomaterial was obtained in the process of treatment of a carbon-containing gas mixture by a high-voltage plasma of atmospheric pressure in a plasma-chemical reactor, the diagram of which is presented in Fig. 1. The initial material was a mixture of a natural gas (methane) with air in the volume ratio of about 2:5. This mixture was transported through the combustion zone of a high-voltage electric discharge in the reactor. The voltage across the electrodes of the discharge gap was 2.4 kV and the discharge current was 100 mA. In the discharge zone (zone I in Fig. 1) the reaction of partial oxidation and decomposition of methane was initiated by thermal heating. This reaction led to the formation of hydrogen, carbon oxide, and, in the long run, a carbon deposit on the hot metallic walls of the deposition zone of the reactor (zone II in Fig. 1). This zone represents a clearance between the cylindrical body of the reactor and the central body made from a stainless steel. The

A. V. Luikov Heat and Mass Transfer Institute, National Academy of Sciences of Belarus, 15 P. Brovka Str., Minsk, 220072, Belarus. Translated from Inzhenerno-Fizicheskii Zhurnal, Vol. 81, No. 1, pp. 137–146, January–February, 2008. Original article submitted February 8, 2007.

1062-0125/08/8101-0145©2008 Springer Science+Business Media, Inc.

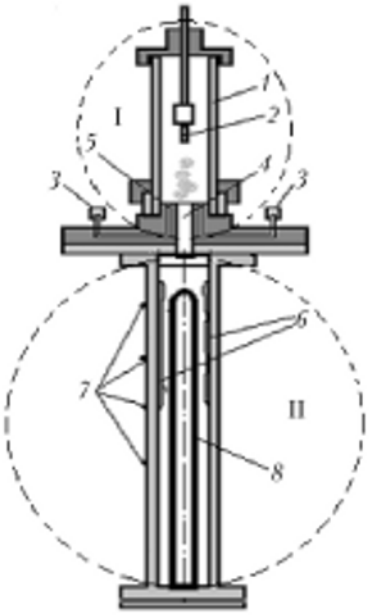

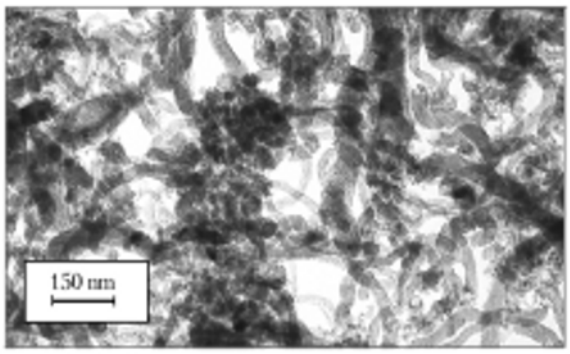

Fig. 1. Scheme of a reactor: I) discharge zone; II) cooling zone; 1) quartz tube; 2) cathode; 3) gas-mixture input; 4) anode hole; 5) anode; 6) carbon material collected; 7) thermocouples; 8) central body.

Fig. 2. Sample of the carbon material produced on the setup (TEM photography).

deposit was periodically collected from the walls of the deposition zone for analysis and further use. In the process of experiment, we measured the flow rates of the gases, the distribution of the reactor-wall temperature along the flow, the composition of the output gases, and the mass of the deposit collected from different parts of the reactor. The typical flow rate of the initial gas mixture was equal to ~680 liters/h. The setup used provided a rate of production with respect to the deposit equal to 4–7 g/h, depending on the experimental conditions. Figure 2 shows a TEM photography of the material obtained on this setup.

Formulation of the Problem. The effect of thermophoresis plays a great role in many technological processes of gas-phase chemical cooling [4–7]. In particular, this effect is widely used in the production of optical fibers [6, 7]. The deposition of nanoparticles from the gas phase on an isothermic plane surface under the action of thermophoresis and the Brownian motion was considered in [8].

As is known [9, 10], the thermophoresis represents a drift of micro- or nanoparticles, suspended in a non-isothermal carrying gas, under the action of a temperature gradient. An elementary molecular-kinetic explanation of this phenomenon is as follows. The momentum obtained by a particle as a result of its collision with fast gas molecules on the hot side is larger than the momentum obtained by this particle from slower molecules on the cold side. Hence, the particle is subjected to the action of the resulting force directed oppositely to the temperature gradient. Under the action of this force, the particle drifts relative to the carrying gas with a constant velocity that, according to the molecular-kinetic theory, is determined as

$$\mathbf{V}_t = -k\frac{\nu}{T}\nabla T. \qquad (1)$$

Here and below the temperature is expressed in kelvins.

The molecular-kinetic theory of gases gives the dependence of the thermophoresis constant on the Knudsen number Kn [10], from which it follows that this constant tends to unity in the free-molecular regime (Kn >> 1).

On the assumption that the carrying gas and the "gas" of particles are mutually penetrating continua, it may be suggested that, if the velocity field of the carrying gas $\mathbf{v}$ is known, the velocity field of the particle gas is equal to $\mathbf{v} + \mathbf{V}_t$. Then the continuity equation for the particle gas will have the form [11]

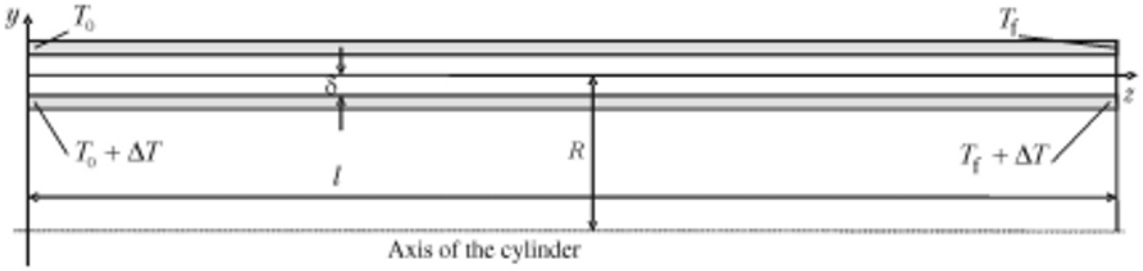

Fig. 3. Geometry of the problem.

$$\frac{\partial \varphi}{\partial t} + \operatorname{div}(\varphi(\mathbf{v} + \mathbf{V}_t)) = 0 . \tag{2}$$

We will simulate the heat and mass transfer in the ring-shaped clearance between the cylindrical wall and the central body in the cooling zone of the reactor on the assumption that $\delta << R$. In this case, the curvature of the gap can be disregarded and considered as a plane channel. The geometrical parameters of the clearance and the coordinate system are presented in Fig. 3. Moreover, it will be assumed that the mass concentration of the particles in the carrying gas is small (in our experiments it comprises 3%); therefore, all the properties of the medium will be considered as independent of the concentration and corresponding to the properties of a pure gas. With these assumptions, the equation of convective heat transfer in the above-described geometry will take the form [12]

$$\tilde{\rho}(T) C_p \hat{U}_z(\tilde{y}, \tilde{z}) \frac{\partial T}{\partial \tilde{z}} = \lambda \frac{\partial^2 T}{\partial \tilde{y}^2} . \tag{3}$$

According to the experimental data, the thermal boundary conditions are defined by the temperature of the clearance walls, decreasing linearly along the z direction. Therefore, the temperatures of the outer wall (the upper wall in Fig. 3) and the inner wall will be equal to

$$T_{b1}(\tilde{z}) = T_f + (T_0 - T_f)\left(1 - \frac{\tilde{z}}{l}\right), \quad T_{b2}(\tilde{z}) = T_f + (T_0 - T_f)\left(1 - \frac{\tilde{z}}{l}\right) + \Delta T . \tag{4}$$

Let us substitute (1) into (2) and write, based on the above assumptions, the equation, obtained for the stationary case, in the geometry presented in Fig. 3. As a result, we obtain the equation for the mass transfer of particles

$$\hat{U}_z(\tilde{y}, \tilde{z}) \frac{\partial \varphi}{\partial \tilde{z}} = k \frac{\partial}{\partial \tilde{y}} \left(\frac{\nu \varphi}{T} \frac{\partial T}{\partial \tilde{y}} \right) - \varphi \frac{\partial \hat{U}_z(\tilde{y}, \tilde{z})}{\partial \tilde{z}} . \tag{5}$$

The velocity profile is assumed to be a developed paraboloid in the case where the velocity amplitude decreases at a constant flow rate as a result of an increase in the particle density along the flow because of the linear change in its temperature. Let the temperature dependence of the particle density have the form

$$\hat{\rho}(T) = \frac{\rho_f T_f}{T} . \tag{6}$$

Since

$$\Delta T << T_0 - T_f \quad \text{and} \quad \Delta T_m << T_0 - T_f , \tag{7}$$

only the dependence of the mixture temperature, averaged over the cross section of the cylinder, on the longitudinal coordinate will be taken into account in (6). Under the external conditions defined by (4), this temperature changes

also linearly. The indicated dependence can be written, in view of (7), in the form of (4). Then, from (6) we find the particle density as a function of $\tilde{z}$:

$$\hat{\rho}\,(\tilde{z}) = \frac{\rho_{\mathrm{f}} T_{\mathrm{f}}}{T_{\mathrm{f}} + (T_0 - T_{\mathrm{f}})\left(1 - \dfrac{\tilde{z}}{\delta}\right)}. \tag{8}$$

In accordance with the aforesaid, the velocity field of the particle flow will be defined as

$$\hat{U}\,(\tilde{y}, \tilde{z}) = \frac{3}{2}\, U_{\mathrm{av}}\,(\tilde{z})\left(1 - \left(\frac{\tilde{y}}{\delta}\right)^2\right). \tag{9}$$

The multiplier $3/2$ in (9) is obtained from the condition

$$\int_{-\delta}^{\delta} \hat{U}_z\,(\tilde{y}, \tilde{z})\, d\tilde{y} = U_{\mathrm{av}}\,(\tilde{z})\,.$$

Then, from the condition of conservation of the mass flow rate G it follows that

$$G = 4\pi R \delta \hat{\rho}\,(\tilde{z})\, U_{\mathrm{av}}\,(\tilde{z})\,. \tag{10}$$

From (7) and (10) we obtain

$$U_{\mathrm{av}}\,(\tilde{z}) = \frac{G}{4\pi} \frac{T_{\mathrm{f}} + (T_0 - T_{\mathrm{f}})\left(1 - \dfrac{\tilde{z}}{\delta}\right)}{R T_{\mathrm{f}} \rho_{\mathrm{f}} \delta} \tag{11}$$

in this case, (9) take the form

$$\hat{U}_z\,(\tilde{y}, \tilde{z}) = \frac{3}{8\pi} \frac{T_{\mathrm{f}} + (T_0 - T_{\mathrm{f}})\left(1 - \dfrac{\tilde{z}}{\delta}\right)}{R T_{\mathrm{f}} \rho_{\mathrm{f}} \delta} \left(1 - \left(\frac{\tilde{y}}{\delta}\right)^2\right). \tag{12}$$

The expression $\dfrac{\nu}{T}$ in (5) can be represented with the use of (6) in the following form:

$$\frac{\nu}{T} = \frac{\mu}{\hat{\rho}\,(T)\, T} = \frac{\mu}{\rho_{\mathrm{f}} T_{\mathrm{f}}}\,. \tag{13}$$

Since the viscosity μ depends on the temperature much weaker than ν, the quantity defined by (13) can be considered as a constant. Let us rewrite system (3), (5) with the use of (7), (12), and (13) as

$$\frac{3}{8} \frac{G \rho_{\mathrm{f}} C_p}{\pi \rho_{\mathrm{f}} \delta} \left(1 - \left(\frac{\tilde{y}}{\delta}\right)^2\right) = \lambda \frac{\partial^2 T}{\partial \tilde{y}^2}\,, \tag{14}$$

$$\frac{3}{8} \frac{G}{\pi \rho_{\mathrm{f}} \delta} \left(1 + \frac{T_0 - T_{\mathrm{f}}}{T_{\mathrm{f}}} \left(1 - \frac{\tilde{z}}{\delta}\right)\right)\left(1 - \left(\frac{\tilde{y}}{\delta}\right)^2\right) = k \frac{\mu}{\rho_{\mathrm{f}} T_{\mathrm{f}}} \frac{\partial}{\partial \tilde{y}} \left(\varphi \frac{\partial T}{\partial \tilde{y}}\right) + \frac{3}{8} \frac{G}{\pi \rho_{\mathrm{f}} \delta^2} \frac{T_0 - T_{\mathrm{f}}}{T_{\mathrm{f}}} \left(1 - \left(\frac{\tilde{y}}{\delta}\right)^2\right) \varphi\,. \tag{15}$$

The boundary conditions for the system of equations (14), (15) are as follows:

$$T(\delta, \tilde{z}) = T_{b1}(\tilde{z}), \quad T(-\delta, \tilde{z}) = T_{b2}(\tilde{z}), \quad \varphi(\tilde{y}, 0) = \varphi_0. \tag{16}$$

Let us introduce the dimensional variables

$$z = \frac{\tilde{z}}{l}, \quad y = \frac{\tilde{y}}{\delta}, \quad \vartheta = \frac{T - T_f}{T_0 - T_f}, \quad \Phi = \frac{\varphi}{\varphi_0}, \quad U = \frac{\hat{U}}{U_{av}}. \tag{17}$$

Equations (12), (14), and (15) can be rewritten, in view of (17), as

$$U(y, z) = \frac{3}{2}(\vartheta^{\times} + (1 - z))(1 - y^2), \tag{18}$$

$$\frac{3}{2}(1 - y^2) = \frac{\chi}{\mathrm{Pe}} \frac{\partial^2 \vartheta}{\partial y^2}, \tag{19}$$

$$\frac{\partial}{\partial z}\left(\frac{3}{2}(\vartheta^{\times} + (1 - z))(1 - y^2)\Phi\right) = \frac{k\chi}{\mathrm{Re}} \frac{\partial}{\partial y}\left(\Phi \frac{\partial T}{\partial y}\right), \tag{20}$$

where the following designations are used:

$$\vartheta^{\times} = \frac{T_f}{T_0 - T_f}; \quad \mathrm{Pe} = \frac{GC_p}{4\lambda\pi R} \equiv \frac{U_{av}\rho C_p \delta}{\lambda}; \quad \mathrm{Re} = \frac{G}{4\mu\pi R} \equiv \frac{U_{av}\rho\delta}{\mu}; \quad \chi = \frac{l}{\delta}. \tag{21}$$

The boundary conditions (4) and (16) are transformed into the dimensionless form:

$$\vartheta(1, z) = 1 - z, \quad \vartheta(-1, z) = 1 + \vartheta^{+} - z, \quad \Phi(0, y) = 1, \tag{22}$$

where $\vartheta^{+} = \dfrac{\Delta T}{T_0 - T_f}$. Relations (18)–(22) represent a mathematical model of the process being investigated.

Solution of the Problem. It is easy to show that the equation of convective heat exchange (18) with the two first boundary conditions (22) is solved as

$$\vartheta(y, z) = \frac{\mathrm{Pe}}{\chi}\left(\frac{y^4}{8} - \frac{3y^2}{4} + \frac{5}{8}\right) + \frac{\vartheta^{+}}{2}(1 - y) + 1 - z. \tag{23}$$

Substituting this solution into (20) and making some rearrangements with allowance for the fact that Pe = Re Pr, we obtain

$$(\vartheta^{\times} + 1 - z)\frac{\partial \Phi}{\partial z} - \frac{k\,\mathrm{Pr}}{1 - y^2}\left(\frac{y^3}{3} - y - \frac{1}{3}\frac{\chi}{\mathrm{Pe}}\vartheta^{+}\right)\frac{\partial \Phi}{\partial y} = (1 - k\,\mathrm{Pr})\,\Phi. \tag{24}$$

The equation of characteristics for the uniform side of Eq. (24) has the form

$$\frac{1}{\vartheta^{\times} + 1 - z}\frac{\partial z}{\partial y} = -\frac{1 - y^2}{k\,\mathrm{Pr}\left(\dfrac{y^3}{3} - y - \dfrac{1}{3}\dfrac{\chi}{\mathrm{Pe}}\vartheta^{+}\right)}. \tag{25}$$

The solution $\tilde{z}_o(y)$ of this equation with the boundary condition $\tilde{z}_o(y) = z_0$ for each z_0 defines the paths of the particles falling on the outer wall of the clearance at the point with a coordinate $z = z_0$. Analogously the solution $\tilde{z}_i(y)$ of the indicated equation with the boundary condition $\tilde{z}_i(-1) = z_0$ gives the paths of the particles falling on the inner wall of the clearance at the point with a coordinate $z = z_0$. Solving (25) with indicated boundary conditions, we obtain equations for the two above-described families of particle paths:

$$\tilde{z}_o(y) = \vartheta^{\times} + 1 - (\vartheta^{\times} + 1 - z_0)\left(\frac{2 + \frac{2\chi}{\mathrm{Pe}}\vartheta^{+}}{-y^3 + 3y + \frac{\chi}{\mathrm{Pe}}\vartheta^{+}}\right)^{\frac{1}{k\mathrm{Pr}}}, \tag{26}$$

$$\tilde{z}_i(y) = \vartheta^{\times} + 1 - (\vartheta^{\times} + 1 - z_0)\left(\frac{-2 + \frac{2\chi}{\mathrm{Pe}}\vartheta^{+}}{-y^3 + 3y + \frac{\chi}{\mathrm{Pe}}\vartheta^{+}}\right)^{\frac{1}{k\mathrm{Pr}}}. \tag{27}$$

In the case where there is no need to find the particle-density field in the clearance and it is necessary to determine only the characteristics of the particles deposited on its walls, all information of interest for us can be obtained from the analysis of the equations for the particle paths (equations of characteristics) (26), (27). Thus, the amount of the carbon material deposited on each wall of the clearance can be calculated in the following way. Assuming that $z_0 = 1$ in (26) and (27) and that the left side of these equations is equal to zero, we will obtain two cubic equations in y for two families of particle paths:

$$-y^3 + 3y + \frac{\chi}{\mathrm{Pe}}\vartheta^{+} - \left(\frac{\chi}{\mathrm{Pe}}\vartheta^{+} - 2\right)\left(\frac{\vartheta^{\times}}{\vartheta^{\times} + 1}\right)^{k\mathrm{Pr}} = 0, \tag{28}$$

$$-y^3 + 3y + \frac{\chi}{\mathrm{Pe}}\vartheta^{+} - \left(\frac{\chi}{\mathrm{Pe}}\vartheta^{+} + 2\right)\left(\frac{\vartheta^{\times}}{\vartheta^{\times} + 1}\right)^{k\mathrm{Pr}} = 0. \tag{29}$$

The roots of these equations y_i (for (28)) and y_o (for (29)) fall within the internal $(-1, 1)$ and determine the transverse coordinate of the critical particle paths, i.e., the paths that end, at the output cross section of the clearance, at the inner and outer walls respectively. All the particles, the transverse position of which in the input cross section of the clearance satisfy the conditions $y \le y_i$ and $y \ge y_o$, fall on the walls of the clearance, i.e., they are deposited under the conditions of 100% adhesion. The other particles are carried out by the flow. It follows herefrom that the fraction of deposited particles is calculated as

$$d = d_i + d_o, \tag{30}$$

where

$$d_o = \frac{\int_{\delta}^{y_o} \tilde{U}_z(\tilde{y}, 0)\, 2\pi (R + \tilde{y})\, d\tilde{y}}{\int_{-\delta}^{\delta} \tilde{U}_z(\tilde{y}, 0)\, 2\pi (R + \tilde{y})\, d\tilde{y}} = \frac{\int_{y_o}^{1} (1 - y^2)(R_d + y)\, dy}{\int_{-1}^{1} (1 - y^2)(R_d + y)\, dy}$$

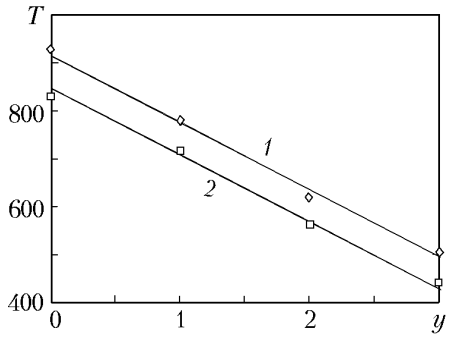

Fig. 4. Temperature of the clearance walls: 1) inner wall; 2) outer wall. T, ^{o}C.

$$= \frac{3}{4R_{\mathrm{d}}}\left(\frac{2}{3}R_{\mathrm{d}} + \frac{1}{4} - R_{\mathrm{d}}\left(y_{\mathrm{o}} - \frac{y_{\mathrm{o}}^3}{3}\right) - \left(\frac{y_{\mathrm{o}}^2}{2} - \frac{y_{\mathrm{o}}^4}{4}\right)\right); \tag{31}$$

$$d_{\mathrm{i}} = \frac{\int\limits_{-\delta}^{\tilde{y}_{\mathrm{i}}} \tilde{U}_z(\tilde{y}, 0)\, 2\pi\,(R+\tilde{y})\, d\tilde{y}}{\int\limits_{-\delta}^{\delta} \tilde{U}_z(\tilde{y}, 0)\, 2\pi\,(R+\tilde{y})\, d\tilde{y}} = \frac{\int\limits_{-1}^{y_{\mathrm{i}}} (1-y^2)\,(R_{\mathrm{d}}+y)\, dy}{\int\limits_{-1}^{1} (1-y^2)\,(R_{\mathrm{d}}+y)\, dy}$$

$$= \frac{3}{4R_{\mathrm{d}}}\left(\frac{2}{3}R_{\mathrm{d}} - \frac{1}{4} + R_{\mathrm{d}}\left(y_{\mathrm{o}} - \frac{y_{\mathrm{o}}^3}{3}\right) + \left(\frac{y_{\mathrm{o}}^2}{2} - \frac{y_{\mathrm{o}}^4}{4}\right)\right). \tag{32}$$

As is seen, in the relations presented the mass of the deposited particles is calculated with account for the cylindrical geometry of the clearance. Thus, the plane-geometry approximation is used only for calculating the velocity and temperature profiles. The mass transfer is determined for the cylindrical geometry. In this case, the mass of the carbon material deposited on the walls of the reactor is equal to

$$m_{\mathrm{o}} = G c_{\mathrm{C}}^0 d_{\mathrm{o}} \tau\,, \quad m_{\mathrm{i}} = G c_{\mathrm{C}}^0 d_{\mathrm{i}} \tau\,, \tag{33}$$

where $c_{\mathrm{C}}^0 = \dfrac{\varphi_0 T_{\mathrm{f}}}{\rho_{\mathrm{f}} T_0}$ is the mass concentration of the particles at the input cross section.

The relations obtained allow one to compare theoretical predictions with experimental data.

Experimental Results and Comparison of Them with the Theory. At the moment only two experiments have given complete sets of measurement data, necessary for the performance of calculations by the above-presented theoretical relations; the analogous experiments, carried out earlier, were oriented to the solution of other problems. We plan to conduct a special series of experiments for the purpose of investigating the postulated developed in more detail.

Figure 4 presents the temperature distribution along the walls of the clearance, measured in experiment No. 1 (Table 1). The points are experimental values of the temperature at the clearance walls and the lines are linear approximations of the temperature distribution over these walls, determined with the use of (3) and (4). The approximation parameters are T_0 = 828^{o}C, T_{f} = 430^{o}C, and ΔT = 67.5^{o}C. As is seen, the supposition that the temperature distribution is linear in character, adopted in the above-described model, is fulfilled with a sufficient accuracy. The initial mixture consists of methane and air; therefore, its main components are methane, nitrogen, and oxygen. The above-presented parameters of the temperature-distribution approximation allow one to calculate the dimensionless parameters used in the model and determined in (21) and (22): $\vartheta^{\times}$ = 1.682, ϑ^{+} = 0.1615. The volumetric flow rates of

TABLE 1. Comparison of Experimental and Calculation Data on the Carbon-Deposit Mass

Parameters	Experiment No. 1		Experiment No. 2	
	Measurements	Calculation	Measurements	Calculation
m_i, g	1.36	2.04	1.40	1.29
m_o, g	4.24	5.17	4.47	4.39
$m_o + m_i$, g	5.60	7.21	5.87	5.68
m_i/m_o	0.321	0.394	0.311	0.293
d	—	0.279	—	0.229

the mixture components in the experiment being considered were W_a = 480 liters/h for air, W_{CH_4} = 203 liters/h for methane, and W = 683 liters/h for the total flow. This relation between the components provides the following volume (molar) concentrations of the mixture components: $X_{CH_4} = 0.297$, $X_{O_2} = 0.148$, $X_{N_2} = 0.555$.

To compare theoretical results and experimental data, it is necessary to calculate the amount of the carbon material deposited on the walls of the deposition zone by the relations presented (see (33)) and the above relations. However, to do this, it is necessary to know the mass concentration of the carbon particles at the input to the deposition zone c_C^0. This quantity can be calculated by the chemical balance of the atoms participating in the reaction with the use of experimental data on the composition of the initial mixture and the composition of the gaseous reaction products at the output of the reactor. As a result of the gas-chromatographic analysis of the gaseous reaction products, we obtained the following their composition (the data presented were averaged over the results of several experiments): $X_{CH_4}^g = 0.05$, $X_{H_2}^g = 0.345$, $X_{N_2}^g = 0.4213$, $X_{CO}^g = 0.465$ (this analysis was carried out without regard for the presence of water and carbon vapors in the mixture; it is suggested that these vapors are contained in the form of nanoparticles in the mixture).

Thus, the chemical transformations in the reactor proceed by the following gross scheme

$$N_2 + O_2 + CH_4 \rightarrow N_2 + C + CH_4 + H_2 + CO + H_2O\,.$$

As follows from this scheme, nitrogen is a passive admixture because it does not form, in the long run, any compounds; therefore, its flow rates at the input and output of the reactor should be equal. This makes it possible to calculate the volumetric W_i^0 and molar w_i^0 flow rates of the gaseous components of the reacted mixture by their known concentrations:

$$W_i^0 = W_{N_2}\frac{X_i^g}{X_{N_2}^g}\,, \quad w_i^0 = \frac{W_i^0}{V_{ml}}\,, \tag{34}$$

where $v_{ml} = 22.4\cdot10^{-3}$ m^3/mole is the molar volume of the gases and i = CH_4, H_2, N_2, CO.

From the condition of balance of atoms of individual reacting substances the relations, to which the volumetric (molar) flow rates of the components (oxygen, hydrogen, and carbon) should satisfy, follow:

$$2W_{O_2} = W_{CO}^0 + W_{H_2O}^0\,, \quad 4W_{CH_4} = 4W_{CH_4}^0 + 2W_{H_2}^0 + 2W_{H_2O}^0\,, \quad W_{CH_4} = W_C^0 + W_{CH_4}^0 + W_{CO}^0\,. \tag{35}$$

The flow rates of the remaining components, i.e., W_C^0 and $W_{H_2O}^0$ can be calculated with the use of (35) and by the flow rates of the gas components determined from (34); the last-mentioned quantity can be calculated by the two independent methods. Actually, from (35) we have

$$W_{H_2O}^0 = 2W_{O_2} - W_{CO}^0\,, \quad W_{H_2O}^0 = 2W_{CH_4} - 2W_{CH_4}^0 - W_{H_2}^0\,, \quad W_C^0 = W_{CH_4} - W_{CH_4}^0 - W_{CO}^0\,. \tag{36}$$

The rates of the water-vapor flow, calculated by the two first formulas of (36) differ by no more than 5% (10% for experiment No. 2, Table 1). This points to a satisfactory agreement between the data obtained, which can be consid-

TABLE 2. Molar and Mass Concentrations of the Reacted Gas Mixture

Parameters	CH_4	H_2	N_2	CO	H_2O	C
X^0	0.045	0.313	0.422	0.127	0.093	0.053
c^0	0.038	0.033	0.62	0.187	0.088	0.034

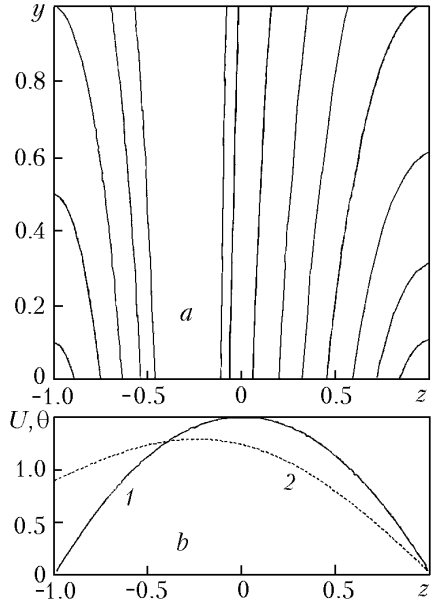

Fig. 5. Particle paths in the clearance (a) and dimensionless profiles of velocity (1) and temperature (2) (b).

ered as evidence that the set of components being considered and their concentrations are adequate to provide a chemical balance of the process being investigated.

The molar flow rates of the mixture components, determined by relations (35) and (36), can be used for calculating the molar concentrations of these components X_i^0. Here, unlike the gas-chromatographic analysis data, we consider the concentrations of the components in the total mixture, i.e., in the mixture containing water vapor and carbon; therefore, the index i takes six different values. The indicated concentrations are calculated as

$$X_i^0 = \frac{w_i^0}{\sum_{j=1}^{6} w_j^0}, \quad i = \mathrm{CH_4},\ \mathrm{H},\ \mathrm{N_2},\ \mathrm{CO},\ \mathrm{H_2O},\ \mathrm{C}. \tag{37}$$

Passing from the molar concentrations to the mass concentrations with the use of standard relations, we can determine the desired value of c_{C}^0. The results of these calculations are presented in Table 2. The concentration of free carbon in the reacted mixture c_{C}^0, determined in this way, can be used for calculating, by relations (31)–(33), the mass of the deposit; the concentrations of the other components are used to determine the physical properties of the mixture.

Using the data on the composition of the mixture reacted and the viscosities of its three main gaseous components, obtained for the average temperature of the clearance walls, we determined the viscosity of the gas medium in the clearance with the use of the Wilke method [13], and calculated the Reynolds and Prandtl criteria: Re = 30.6, Pr = 0.7. As is known [14], the lengths of the initial thermal and hydrodynamic regions are equal to $l_{\mathrm{h}} = 0.2\ \mathrm{Re}\ \delta$ and $l_{\mathrm{t}} = 0.2\ \mathrm{Re\ Pr}\ \delta$. In our case (the geometric dimensions of the channel are $R = 0.0135$ m, $\delta = 0.0035$ m, $l = 0.24$ m), we obtain that the lengths of the initial regions of the channel do not exceed 10% of its total length. This points to the fact that the approximation of a completely developed convective heat exchange, adopted in the mathematical model, can be used here. The characteristics of the process being considered can be calculated by the data presented

in accordance with the theoretical model. The thermophoresis in the free molecular regime, where the particles have sizes of smaller than the mean free path of the molecules in the carrying medium (of the order of 100 nm in our case), is usually calculated with a thermophoresis constant $k = 1$.

Figure 5 shows the particle paths in the clearance and the profiles of the dimensionless velocity $U(y, z)$ and the transverse component of the dimensionless temperature $\theta(y) = \vartheta(y, z) - (1 - z)$, calculated by relations (26), (27) and (18), (21) with the use of the process parameters determined above by the experimental data. As is seen, the temperature profile reaches a maximum inside the clearance; therefore, the temperature gradient near its walls is directed to the axis. Since the thermophoresis force is opposite to the temperature gradient, it causes particles to deposit on both walls. This is evidenced from the configuration of the particle paths: the particle paths that, at the initial cross section, pass near the walls end at the walls of the clearance. The particles found in the central region are carried out by the flow. It is seen that the efficiency of the deposition is small — the fraction of particles carried out by the flow is larger than the fraction of the deposited particles.

Analogous calculations were carried out for experiment No. 2. In this experiment, the flow rate and composition of the mixture supplied into the reactor differed somewhat from those in the previous experiment; which caused changes in the other parameters. The initial data used for calculations of this experiment were the parameters of approximation of the temperature distribution over the walls of the clearance $T_0 = 774^{\circ}$C, $T_f = 466^{\circ}$C, and $\Delta T = 76.2^{\circ}$C; the volumetric flow rates of the mixture components $W_a = 486$ liters/h and $W_{CH_4} = 200$ liters/h; the rate of the total flow $W = 686$ liters/h. The composition of the reacted mixture was determined by the averaged chromatographic-analysis data used for the first experiment. The duration of each of the experiments being considered was 1 h. The masses of the deposited carbon material, calculated by relations (30)–(33) for both experiments, and the corresponding experimental data are presented in Table 1. Comparison of the calculation and experimental data obtained shows that the predictions of the theory described here agree satisfactorily with the available experimental data.

At a later time we plan to conduct a special series of experiments for investigating the postulates developed in the present work in more detail with the use of a modified setup with a cooling zone made in the form of a plane clearance, equipped with external heaters for control of the wall-temperature distribution and a larger number of detectors.

CONCLUSIONS

1. The results of the present work strengthen the hypothesis that thermophoresis plays a great role in the process of transport of carbon clusters to the deposition surface in a flow discharge reactor. This allows the conclusion that carbon is partially deposited in the form of particles on the substrate under the action of the temperature gradient.

2. The structure of these particles (structurized nanomaterials, graphene, or amorphous carbon) and the transformations of the clusters on the metallic surface call for additional investigations.

3. The theoretical model of the process being considered, developed by us, is consistent with experiment and can be used for calculating the parameters of this process and its optimization.

4. The calculation data obtained show that the efficiency of deposition of carbon particles is comparatively low (about 28%), which points to the fact that the process being considered can be further improved for increasing its output.

NOTATION

d, proportion of the deposited particles of all the particles carried out by the flow to the clearance; d_i, proportion of the particles deposited on the inner wall of the clearance; d_o, proportion of the particles deposited on the outer wall of the clearance; c_C^0, mass concentration of the carbon particles at the input to the deposition zone; C_p, isobaric heat capacity of the mixture; G, mass flow rate of the working mixture in the reactor; k, dimensionless thermophoresis constant; Kn, Knudsen number; l_h, length of the initial hydrodynamic region in the channel; l_t, length of the initial thermal region in the channel; l, length of the channel; Pe, Peclet number; Pr, Prandtl number; R, average radius of the clearance; R_d, dimensionless average radius of the clearance; Re, Reynolds number; t, time; T, absolute temperature of the mixture; ΔT_m, maximum temperature drop at the cross section of the flow; ΔT, difference between the temperatures at the input and output cross sections of the flow; $\hat{U}_z$, velocity profile of the flow; $U_{av}(\tilde{z})$, dependence of the

average velocity of the flow on $\tilde{z}$; U, dimensionless velocity of the flow; **v**, vector of the velocity field; V_t, rate of thermophoresis; W_a, W_{CH_4}, and W, volumetric rates of air, methane, and the initial mixture respectively; W_i^0 and w_i^0, molar and mass flow rates of the components of the gaseous mixture reacted; X_{CH_4}, X_{O_2}, and X_{N_2}, volume concentrations of methane, oxygen, and nitrogen in the initial mixture; X_i^0, molar concentration of the ith component in the mixture reacted; y, dimensionless transverse coordinate; y_i and y_o, transverse coordinates of the initial points (at the input cross section of the channel) of the critical paths of the particles falling on the inner and outer walls of the channel respectively at the input cross section; z, dimensionless longitudinal coordinate; $\tilde{z}_o(y)$ and $\tilde{z}_i(y)$, functions defining the particle paths ending at the outer and inner walls of the clearance respectively; δ, half-width of the clearance; λ, heat-conductivity coefficient of the mixture; μ, dynamic viscosity of the mixture; ν, kinematic viscosity of the mixture; ϑ, dimensionless temperature; $\vartheta^\times$, χ, dimensionless parameters determined in (21); $\theta(y)$, transverse component of the dimensionless temperature distribution; λ, heat-conductivity coefficient of the mixture ρ_f, density of the mixture at the output cross section; $\tilde{\rho}(T)$, temperature dependence of the mixture density; τ, duration of an experiment; φ, mass density of particles in the mixture; Φ, dimensionless mass density of particles in the mixture. Subscripts: i, inner; o, outer wall; h, hydrodynamic; t, thermophoresis; d, clearance; m, maximum; av, average; a, air; ml, molar; 0, input cross section; f, output cross section; b, boundary (wall); g, gas.

REFERENCES

1. S. S. Pesetskii, S. A. Zhdanok, I. F. Buyakov, S. P. Bogdanovich, A. P. Solntsev, and A. V. Krauklis, On the structure and properties of polyamide 6 modified in a melt by carbon nanomaterials, *Dokl. Nats. Akad. Nauk Belarusi*, **44**, No. 6, 102–107 (2004).
2. S. A. Zhdanok, I. F. Buyakov, A. V. Krauklis, et al., Influence of process parameters upon the properties of carbon nanomaterials synthesized in the electric discharge, *Nonequilibrium Processes in Combustion and Plasma Based Technologies*, Int. Workshop, Minsk (2004), pp. 205–209.
3. V. V. Chesnokov and R. A. Buyanov, Formation of carbon filaments in the process of catalytic decomposition of hydrocarbons on iron-subgroup metals and their alloys, *Usp. Khimii*, **69**, Issue 7, 675–697 (2000).
4. C.-J. Tsai, J.-S. Lin, S. G. Aggarwal, and D.-R. Chen, Thermophoretic deposition of particles in laminar and turbulent tube flows, *Aerosol Sci. Technol.*, **38**, No. 2, 131–139 (2004).
5. L. Talbot, R. K. Cheng, R. W. Scefer, and D. R. Willis, Thermophoresis of particles in a heated boundary layer, *J. Fluid Mech.*, **101**, 737–758 (1980).
6. K. L. Walker, F. T. Geyling, and S. R. Nagel, Thermoforetic deposition of small particles in the modified chemical vapor deposition (MCVD) process, *J. Am. Ceram. Soc.*, **63**, Nos. 9–10, 552 (1980).
7. V. L. Kolpashchikov, Yu. K. Krivosheev, O. G. Martynenko, and A. I. Shnip, Processes of gas-phase deposition in the process of formation of blanks for optical fibers, in: *Heat- and Mass Transfer: Theory and Practical Applications* [in Russian], ITMO AN BSSR, Minsk (1983).
8. S. P. Fisenko and A. I. Shnip, Deposition of nanoparticles on cold substrate from laminar gas flow, in: V. E. Borisenko (Ed.), *Physics*, *Chemistry and Applications of Nanostructures*, World Scientific, Singapore (2003), pp. 291–293.
9. H. Green and W. Lane, *Particulate Clouds*, *Dust*, *Smokes*, *and Mists* [Russian translation], Khimiya, Leningrad (1969).
10. D. V. Derjaguin, Y. I. Rabinovich, A. I. Storozhilov, and G. I. Shcherbina, Measurement of coefficient of thermal slip of gases and thermophoresis velocity of large-size aerosol particles, *J. Colloid Interface Sci.*, **57**, 451 (1978).
11. L. D. Landau and E. M. Lifshitz, *Fluid Dynamics*, Pergamon, London (1987).
12. B. S. Petukhov, *Heat Transfer and Drag in a Laminar Liquid Flow in Tubes* [in Russian], Énergiya, Moscow (1967).
13. R. Reid and T. Sherwood, *The Properties of Gases and Liquids* [Russian translation], Khimiya, Moscow (1971).
14. T. Cebeci and P. Bradshaw, *Physical and Computational Aspects of Convective Heat Transfer* [Russian translation], Mir, Moscow (1987).